Environmental Pollution 338 (2023) 122680

Contents lists available at ScienceDirect

Environmental Pollution

journal homepage: www.elsevier.com/locate/envpol

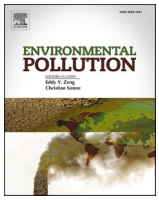

Size-resolved emission rates of episodic indoor sources and ultrafine particle dynamics☆

Su-Gwang Jeong [a], Lance Wallace [b], Donghyun Rim [c,*]

[a] Department of Architectural Engineering, Soongsil University, Seoul, 06978, Republic of Korea
[b] Wallace Research, Santa Rosa, CA, 95409, USA
[c] Department of Architectural Engineering, Pennsylvania State University, University Park, PA, 16802, USA

ARTICLE INFO

Keywords:
Indoor air quality
Sources strength
Nanoparticles
Coagulation
Deposition
Size distribution

ABSTRACT

Indoor airborne ultrafine particles (UFPs) are mainly originated from occupant activities, such as candle burning and cooking. Elevated exposure to UFPs has been found to increase oxidative stress and cause DNA damage. UFPs originating from indoor sources undergo dynamic aerosol transformation mechanisms. This study investigates the dynamics of UFPs following episodic indoor releases of the six distinct emission sources: 1) candle, 2) gas stove, 3) clothes dryer, 4) tea & toast, 5) broiled fish, and 6) incense. Based on the analytical model of aerosol dynamic processes, this study reports size-resolved source emission rates along with relative contributions of coagulation, deposition, and ventilation to the particle size distribution dynamics. The study findings indicate a significant variation in the geometric mean diameter (GMD) and size-resolved number concentration over time for the sources that emit a substantial amount of UFPs smaller than 10 nm. As the emission progresses, the UFP number concentrations increase in a log-normal distribution, while the GMD shows a tendency to increase over time. The observed result suggests that coagulation can have a considerable impact on UFP number concentration and size, even during the indoor UFP emission. The estimated emission rates of the six indoor sources appear to follow a log-normal distribution while the emission rate ranges from 10^7 min^{-1} to 10^{12} min^{-1}. The indoor UFP concentration and size distribution dynamics are substantially affected by the interplay of the three aerosol loss mechanisms that compete with each other, and this impact varies according to the source type and the indoor environmental conditions. Ultimately, using the aerosol transformation mechanisms examined in this study, researchers can refine exposure assessment for epidemiological studies on indoor ultrafine particles.

1. Introduction

Indoor airborne ultrafine particles (UFPs, <100 nm) have been discovered to be toxic to human health and associated with several negative health impacts, including inflammatory, cardiovascular, and respiratory diseases (Li et al., 2021; Ohlwein et al., 2019; Slezakova et al., 2020). As people spend most of their lifetime in enclosed buildings, human exposure to UFPs are largely attributed to indoor emission sources (Amouei Torkmahalleh et al., 2022; Koivisto et al., 2019; Nazaroff, 2008; Ott et al., 2021). Indoor occupant activities such as use of candles and cooking are mostly episodic, but can lead to intermittently high airborne particle concentrations (Bhangar et al., 2011; Hussein et al., 2006; Jeong et al., 2021; Li et al., 2020; Rim et al., 2012; Wang et al., 2018).

Once emitted from indoor sources, UFPs undergo dynamic aerosol transformation processes including evaporation, condensation, coagulation, and deposition (Adeniran et al., 2019; Hinds, 1982; Hussein et al., 2009; Koivisto et al., 2012; Patel et al., 2021; Wallace et al., 2019). These processes can alter particle size distribution and concentration over time, affecting human exposure profiles. In particular, when particle number concentration is high in an indoor space, coagulation can notably influence the UFP loss mechanism. Particles aggregate and grow larger during the coagulation process, which leads to the production of bigger particles and the depletion of smaller particles. Such coagulation process shifts the geometric mean diameter (GMD) in the UFP size distribution towards a larger size while decreasing the total UFP number concentration over time, although the influence varies with emission period, emission strength and source type (Anand et al., 2016; Nazaroff

☆ This paper has been recommended for acceptance by Sumin Kim

* Corresponding author. Pennsylvania State University, University Park, PA, 16802, USA
E-mail address: drim@psu.edu (D. Rim).

https://doi.org/10.1016/j.envpol.2023.122680
Received 20 March 2023; Received in revised form 17 August 2023; Accepted 1 October 2023
Available online 9 October 2023

and Cass, 1989; Wallace, 2006; Wallace et al., 2008; Zhao et al., 2015).

Several previous studies have reported indoor aerosol dynamic behaviors due to deposition, ventilation, and emission sources associated with different types of indoor source activities. Patel et al. (2021) characterized deposition rates specific to a test house (House Observations of Microbial and Environmental Chemistry; HOMEChem) and reported emission rates of particles <500 nm. They found that UFPs dominated emission rates for number-based concentrations, whereas large particles (>100 nm) were responsible for mass-based emission rates. They also demonstrated that coagulation substantially influenced the total UFP number concentration and that an increase in air exchange rate led to almost linear reduction of number-based PM exposure (Patel et al., 2021). Yu et al. (2013) investigated the size-resolved coagulation loss rate to deposition loss for five different geometric mean diameters (i.e., 5.4, 23, 120, 537, and 2680 nm) through theoretical analysis, with the same total particle number concentration (1.0×10^4 cm^{-3}) and the same geometric standard deviation (GSD) ($\sigma_g = 1.5$). The theoretical analysis method was validated by experimental tests in a ventilated laboratory chamber. They observed significant dependence of the ratio of coagulation rates to deposition on the particle size distribution and number concentration (Yu et al., 2013). Zai et al. (2006) introduced a model-based method for determining the size-specific particle number and mass emission factors during candle combustion, characterized by three distinct burning modes. Candle emissions were linked to three varying burning modes defined as steady burning, unsteady burning, and smoldering in the study. The emission rates were estimated as (4.05 ± 0.73) $\times 10^{12}$ min^{-1} for the steady burning, (1.49 ± 0.32) $\times 10^{12}$ min^{-1} for the unsteady burning, and (1.55 ± 0.23) $\times 10^{11}$ min^{-1} for the smoldering mode. This model-based method help understand size-specific dynamic behavior by accounting for particle growth due to coagulation (Zai et al., 2006). Zhang et al. (2014) conducted an analysis of fine particle ($PM_{2.5}$) and UFP emissions from microwaving popcorn and analyzed influential factors. Each pre-packed popcorn bag was cooked in a microwave oven enclosed within a stainless-steel chamber for 3 min. During popping, the concentration of total particle number rapidly increased from the background level of around 0.3×10^3 cm^{-3} to a peak concentration above 300×10^3 cm^{-3}. Similarly, the mass concentration of $PM_{2.5}$ increased sharply from the background level of 1.5 μg/m^3 to a peak concentration around 1500 μg/m^3. However, the peak concentrations of $PM_{2.5}$ mass were observed 1.5–2 min following the peak of the total particle number concentration. This observation indicates that the initial surge in PM primarily took place within the ultrafine size range, and subsequently, these smaller particles aggregate to form larger sizes, which was supported by the size distributions (Zhang et al., 2014). Laiman et al. (2014) investigated changes in particle number concentration within naturally ventilated primary school classrooms resulting from local sources either within or adjacent to the classrooms. This study was conducted in a total of 50 classrooms across 25 urban schools to identify indoor particle sources and quantify their emission and deposition rates. The average particle emission rates from heating, printing, and grilling were (2.51 ± 0.25) $\times 10^{11}$ min^{-1}, (5.17 ± 2.0) $\times 10^{11}$ min^{-1}, and (8.99 ± 6.70) $\times 10^{11}$ min^{-1}, respectively. The average total particle deposition rates for the classrooms were approximately 100 times greater than the air exchange rates, indicating that particle deposition is the primary removal mechanism for particles originating from indoor sources (Laiman et al., 2014). Table S1 presents detailed information on studies related to indoor aerosol emission rates and dynamic behaviors.

Our previous study (Jeong et al., 2021) established an indoor particle dynamic model that can estimate relative contributions of three aerosol transformation processes (coagulation, deposition, and ventilation) to the total particle loss for six source emission events (i.e., candle, gas stove, clothes dryer, toast, broiled fish, incense). However, this study along with most previous studies are limited to the aerosol loss mechanisms only for the particle decay period, and still, very little is known about size-resolved UFP emission rates associated with indoor source activities. In most of previous studies, only the aerosol transformation during the decay period was examined. Therefore, the novelty of this study is the development of a modeling framework that calculates size-resolved emission rates while considering the three dynamic behaviors (i.e., coagulation, deposition, and ventilation) of indoor particles. Given this background, this study has two objectives: 1) to establish an analytical model that predicts particle transformation processes for any indoor emission events during emission and decay periods; and 2) to estimate size-resolved UFP emission rates for common episodic indoor emission sources considering coagulation, deposition, and ventilation.

2. Methods

2.1. Experimental data and indoor emission sources

A modeling framework has been developed to examine indoor particle dynamics of measured datasets from studies in literature (Ogulei et al., 2006; Rim et al., 2012; Wallace, 2006; Wallace et al., 2019; Wallace et al., 2008; Wallace et al., 2004). These datasets contain size-resolved number concentrations for six episodic indoor emission sources (i.e., candle, gas stove, clothes dryer, tea & toast, broiled fish, and incense) in typical residential buildings. These indoor UFP emission sources have been discussed in various studies in literature (Bhangar et al., 2011; Park et al., 2023; Patel et al., 2020; Salthammer et al., 2021; Wierzbicka et al., 2015). Among them, experimental data with six emission sources that had distinct particle size distributions were selected to validate the developed aerosol dynamic model. The experimental data were collected from residential buildings in three locations, namely Santa Rosa (California), Gaithersburg (Maryland), and Reston (Virginia). (See more details on the measurement sites in Table S2).

For the candle test, the measurement data were based on the experiments with taper type candles in a residential office, reported in the paper by Wallace et al. (2019). The experimental setup involved closing the air distribution register and sealing the door with a blanket. The central fan in the building was turned off and the room windows were closed to minimize external influences. To enhance air mixing without directly affecting the particle flow between the source and detectors, a small table fan was used during the test. For the gas stove test, particles were emitted from a gas stove in the kitchen, while all interior doors in the building were open. During the test, the particle size and number concentrations were measured in the master bedroom with a central mixing fan operating at a volume flow rate of 2000 m^3/h for the house volume of 340 m^3 (Wallace et al., 2008). This paper reported the particle size and number concentrations produced by the gas flame and gas stove alone (without pots or food) in 42 experiments. The remaining four source emission data tested herein were from Wallace et al. (2006), which performed measurements in a townhouse consisting of three levels, with an estimated total mixing volume of 400 m^3. Throughout the experiment, the townhouse was occupied by two adults who engaged in various indoor activities, such as cooking (toasting, broiling fish), using a clothes dryer, and burning incense. This study, which measured particles over a period of 37 months, considered a wide range of conditions including different seasons, high and low temperatures, air exchange rates, relative humidity, and various other factors that varied extensively. A total of 18 indoor source emission events were monitored, and among them, the present study selected four sources: clothes dryer (gas-powered), tea (boiling water on a gas burner) & toast (toasting bread in an electric toaster oven) during breakfast, broiled fish (in a gas oven), and burning incense.

Fig. 1 illustrate total number concentrations of UFPs for the six indoor emission sources during the emission and decay periods. In each graph, the vertical blue line indicates the peak total UFP number concentration at the beginning of decay period. It is important to note that the candle, gas stove, broiled fish, clothes dryer, tea & toast, and incense

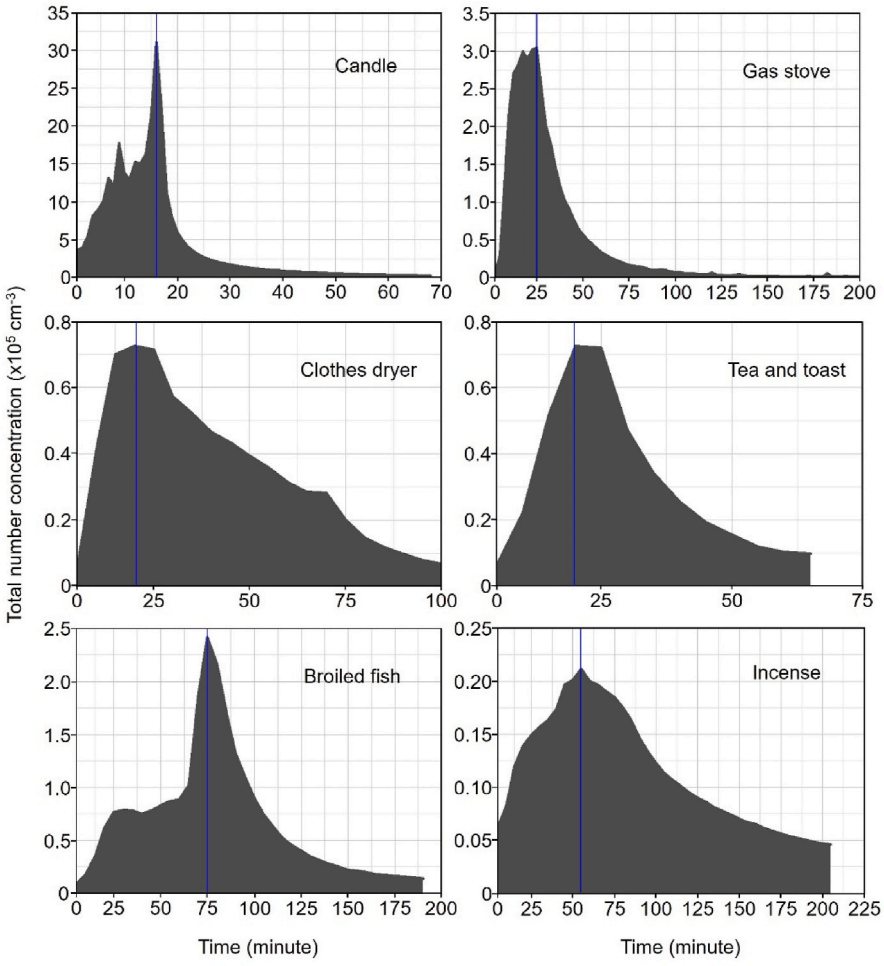

(a) Individual version

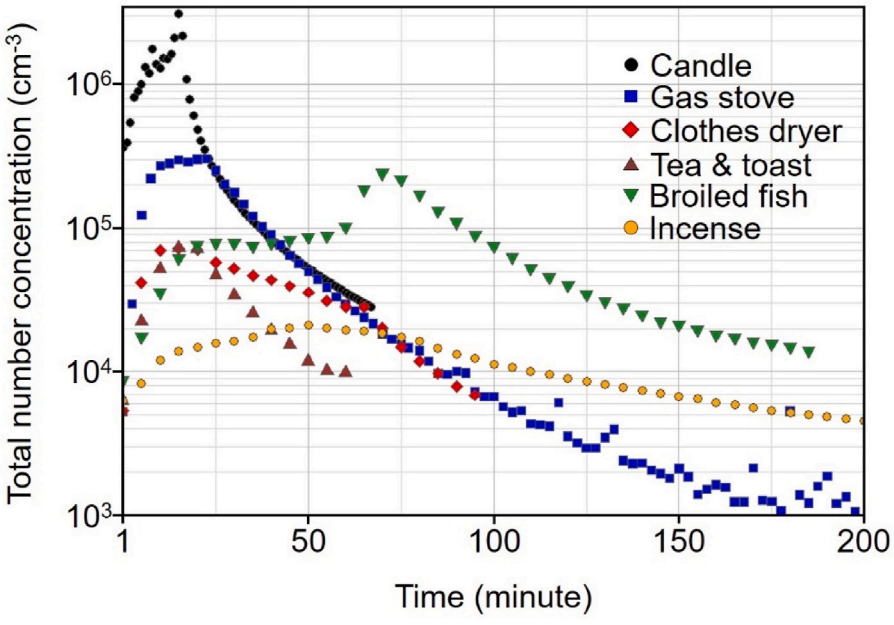

(b) Merged version with a logarithmic scale on the y-axis

Fig. 1. The changes of total UFP number concentrations for the six indoor emission sources during whole monitoring period (a) individual version, (b) merged version with a logarithmic scale on the y-axis.

have the highest total UFP number concentration, listed in order. Each graph indicates a distinct size distribution according to different GMD and GSD for each source type. Note that outdoor-indoor air exchange rate (AER) was investigated using either a tracer gas (SF_6) monitoring system or real-time carbon monoxide sensor in the house. For the six emission sources, the average AER observed during the particle emission and decay periods ranged from 0.04 (±0.01) to 0.50 (±0.03) h^{-1}. Supporting Information contains comprehensive details about air exchange rates and particle size distributions for the emission and decay periods due to all six indoor sources (See Tables S3 and S4).

2.2. Indoor UFP dynamics model

The size-resolved number concentrations and time-varying size distributions for the six indoor emission sources were analyzed using a material-balance model that considered coagulation, deposition, and ventilation, and source emission, as shown in Eq. (1) (Rim et al., 2016).

$$\frac{\partial n(v,t)}{\partial t} = \frac{1}{2}\int_{v_0}^{v-v_0} \beta_{v-\bar{v},\bar{v}} n(v-\bar{v},t) n(\bar{v},t) d\bar{v} - n(v,t)\int_{v_0}^{\infty} \beta_{\bar{v},v} n(\bar{v},t) d\bar{v} - (k+a)n(v,t) + \mathrm{S}(v,t) \Big/ V \quad (1)$$

In the equation, $n(v,t)$ [m^{-3}] represents the particle number concentration for the particle volume [m^3] between v and $v + dv$ at time t [s]; $v - \bar{v}$ and $\bar{v}$ indicate the volumes of the two coagulating particles; v_0 denotes the initial particle volume; v represents the volume of the newly generated particles due to coagulation; β represents the collision rate between two particles (coagulation kernel); k and a are the deposition rate [h^{-1}] and air exchange rate [h^{-1}]; $S(v,t)$ denotes the source emission rate for a specific particle size between v and $v + dv$ at time t [h^{-1}]; and V signifies the volume of the indoor space [m^3].

Particle gain and loss due to coagulation are represented by the first two terms on the right-hand side (RHS), while particle losses caused by deposition and ventilation are counted in the next term on the RHS. The final term on the RHS is the time-dependent source emission for a given size. Note that the emission period varied with source type. The coagulation model considered the coagulation kernel β, which accounted for Brownian diffusion with the Fuchs correction as well as van der Waals and viscous forces (refer to Fig. S1). The Hamaker constant, a coefficient that considers the material-dependent UFP collision potential due to van der Waals force, was assigned a value of 20kBT (where kB is the Boltzmann constant and T is the absolute temperature), which is relevant to indoor organic UFPs (Rim et al., 2016; Rim et al., 2012; Wallace et al., 2019). The coagulation loss rate is dependent on the square of the total number concentration in the space, as it is a second-order loss mechanism. However, to compare the coagulation loss rate over time with other first-order loss mechanisms (i.e., deposition and ventilation), we calculated the first-order equivalent (FOE) coagulation loss rate for specific time intervals using the following formula (Jeong et al., 2021):

$$k_{c,bin}(t) = -ln\left(\frac{N_{0,bin} - N_{c,bin}}{N_{0,bin}}\right) \Big/ t = -ln\left(\frac{initial\ number\ of\ UFPs - number\ of\ coagulation\ loss}{initial\ number\ of\ UFPs}\right) \Big/ t \quad (2)$$

where $k_{c,bin}(t)$ represents the FOE coagulation loss for a given size bin i over time interval t, $N_{0,bin}$ is the initial number concentration for the size bin i, $N_{c,bin}$ is the reduced number concentration due to coagulation for the size bin i.

Furthermore, time-dependent emission rates were calculated while considering the influence of the three aerosol transformation processes during the emission period as shown Eq. (3).

$$S_n(v,t) = C_f n\left(v,t_f\right) - C_i n(v,t_i) + \left[n(v,t)\int_{v_0}^{\infty} \beta_{\bar{v},v} n(\bar{v},t) d\bar{v} - \frac{1}{2}\int_{v_0}^{v-v_0} \beta_{v-\bar{v},\bar{v}} n(v-\bar{v},t) n(\bar{v},t) d\bar{v} + (k+a)n(v,t)\right] \quad (3)$$

where $S_n(v,t)$ represents the emitted number of particles for the particle volume [m^3] between v and $v + dv$ at time t [s], $C_f n(v,t_f)$ and $C_i n(v,t_i)$ represent the number concentration for the particle volumes [m^3] between v and $v + dv$ at the final and initial time steps, respectively.

The source emission rate were calculated based on the number of particles ($S_n(v,t)$) emitted from the source at each time step during the emission period while taking into account the three loss mechanisms. This particle number concentration value is multiplied by the volume of the test room (25.8 m^3 for candles, 340 m^3 for gas stoves, and 400 m^3 for the other four remaining sources), and divided by the time interval specific to each source (1.0 min for candles, 2.5 min for gas stoves, and 5.0 min for the other four remaining sources) to obtain the source emission rates. Finally, the source emission rates calculated at each time step, were averaged to determine the source emission rates during the emission period. The formula for calculation is as follows, and the errors are estimated using the standard error.

$$Source\ emssion\ rates\ \left(min^{-1}\right) = average\left[\frac{(S_n(v,t)) \times volume\ of\ test\ room\ (m^3)}{Time\ interval\ (min)}\right] \quad (4)$$

$$Standard\ Error\ (SE) = \frac{\sigma}{\sqrt{n}} \quad (5)$$

Where, σ is the standard deviation of source emission rates calculated at each time step and n is number of calculated the time step.

2.3. Deposition rates

In this study, an iteration method was applied to calculate the deposition rates of indoor emission sources for each size distribution, considering the time-varying coagulation losses. In a previous study in the literature (Wallace et al., 2019), the iteration method was established and validated based on the multiple decay tests performed in a residential building. A flow diagram iteration model is presented in the SI, however, briefly explaining the iteration method, the initial size-resolved deposition rates were assumed based on the deposition theory presented in the literature (Lai and Nazaroff, 2000; Wallace et al., 2013; Or et al., 2020). Then, for the decay period, particle losses due to the three loss mechanisms were calculated at each time interval (1 min). At each time step, the error between the measured and simulated UFP number concentrations was iteratively compared to estimate the deposition rates that yielded the smallest sum of errors. The estimated deposition rates for different UFP size have specific convergence criterion ($\sum\left|{k_d}^{n+1} - {k_d}^{n}\right| \leq 10^{-2}$), where k_d represents the estimated deposition rates (see Fig. S2). The application of this method yielded size-resolved deposition rates that demonstrated a reasonable level of accuracy. Specifically, the R^2 values of the log-linear curve exhibited a range of 88.3%–96.6% for the data acquired from candle, gas stove, toast, broiled fish, and incense. However, it is important to note that the R^2 value for incense was notably lower at 60.7% (Jeong et al., 2021).

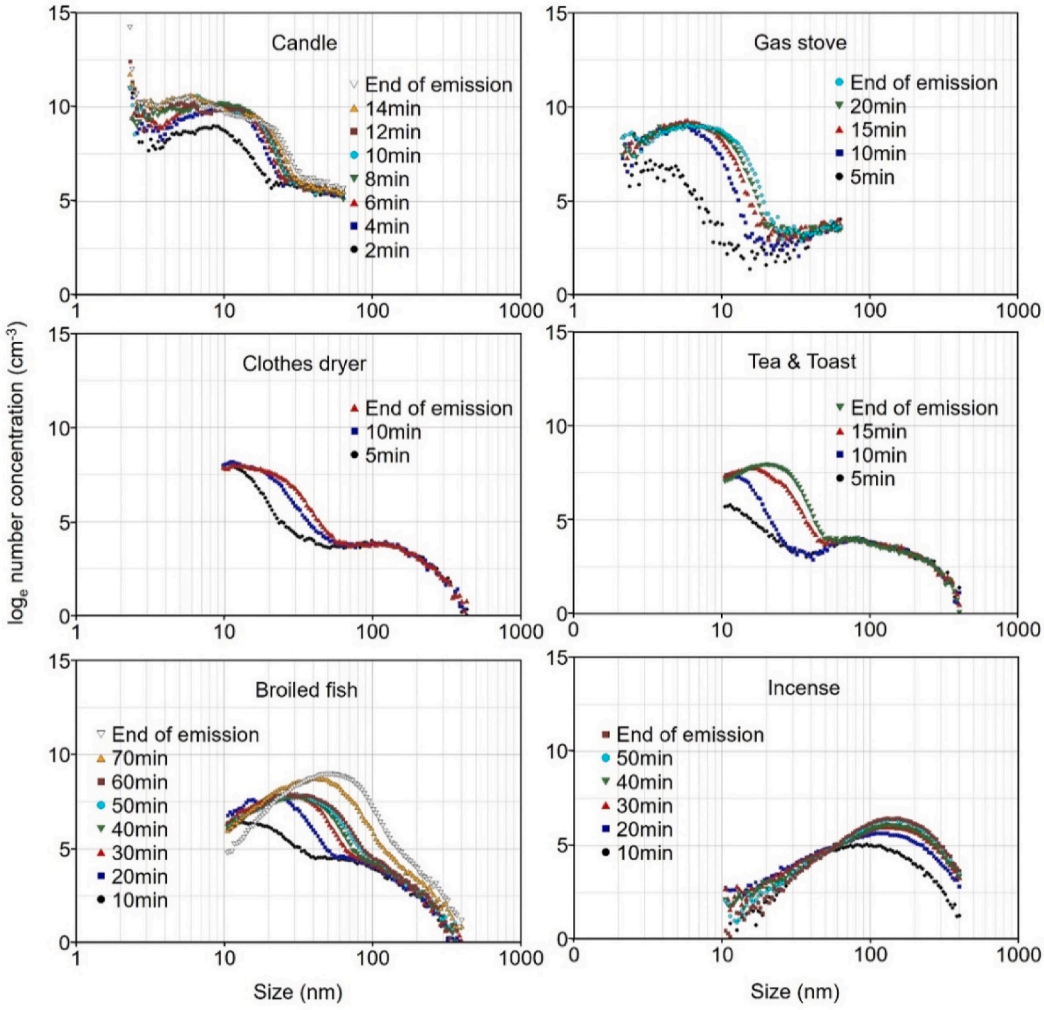

Fig. 2. UFP number concentrations for six indoor sources during emission periods.

3. Results and discussion

3.1. Size distributions due to the indoor emission sources

Fig. 2 shows the changes in particle number concentrations during the emission period for the six indoor emission sources. Note that the emission period varies depending on the emission source type. According to the figure, the particle size distribution notably changes as the emission progresses. Burning a candle resulted in a bimodal log-normal distribution with two peaks in two size ranges: 1) $<$ 3 nm and 2) $\geq$ 3 nm. At the beginning of emission, the highest number concentration (6.14×10^4 cm^{-3}) was observed at 2.33 nm, while at the end of the emission, the highest concentration (37.2×10^3 cm^{-3}) was at 5.71 nm. The study by Glytsos et al. (2010) also reported two modes of concentration of candle burning. They showed that the size distribution during the first 10 min of candle burning was mainly unimodal, but then a second mode was observed in a larger size range.

The gas stove yielded a unimodal log-normal distribution with a majority of the emitted particles $<$10 nm. The highest number concentrations were observed between 2.5 nm and 6.0 nm during the emission. The clothes dryer and tea & toast showed similar size distribution and number concentration, with the GMD in the range of 10–20 nm, although tea & toast showed a larger number concentration at a larger size. In the case of broiled fish, the GMD and the highest number concentration occurred from 11 nm at the beginning to 53 nm at the end of emission. Incense burning released the largest particles among the six emission sources, with the GMD in the range of 94–131 nm. The particle size distribution due to incense showed an increase in GMD from 86 nm at the beginning of emission to 128 nm at the end of emission. As the emission progressed, the number concentration increased in the form of a log-normal distribution, along with the GMD showing a tendency to increase over time.

3.2. Deposition and coagulation loss rates for indoor emission sources

Fig. 3 shows the estimated deposition rates and first-order equivalent coagulation loss rates during the emission period. In general, the deposition rate decreases as the size increases for the size range of $<$70 nm, except for incense for which the deposition rate increases as the size increases. This finding is in agreement with prior research that found the deposition rate greater for smaller UFPs ($<$70 nm) due primarily to Brownian and turbulent diffusion (Gao and Niu, 2007; Lai and Nazaroff, 2000; Siegel and Nazaroff, 2003). In the case of candle and gas stove, relatively high deposition rates ($>$10 h^{-1}) were observed, especially for the small size range ($<$3 nm), while broiled fish showed high deposition rates ($>$10 h^{-1}) at the larger size range (10–18 nm). In the case of clothes dryer, the deposition rates increased in the 10–20 nm range, possibly due to the influence of other possible aerosol transformation mechanisms such as moisture evaporation. The broiled fish case showed a monotonic decrease of deposition rate in the particle size range up to 200 nm, whereas incense shows a monotonic increase from 80 nm to 300 nm. Note that in previous studies, log-normal distributions based on

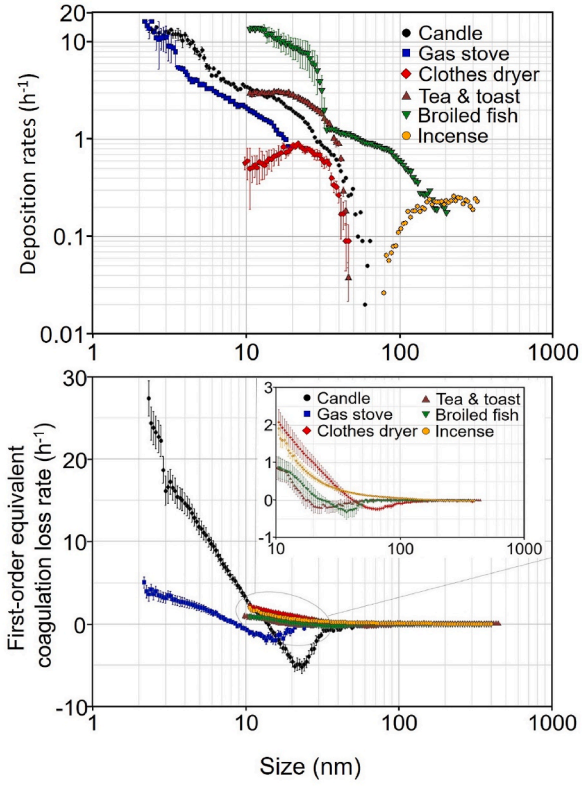

Fig. 3. Deposition rate estimates and first-order equivalent (FOE) coagulation loss rates.

the measurement of particles >10 nm suggest that clothes dryers and broiled fish are expected to have relatively lower concentrations of particles (<10 nm) (Jeong et al., 2021). However, if particle number concentrations below 10 nm are measured to be high, the deposition and coagulation loss rates of broiled fish and clothes dryers could potentially increase significantly.

This trend suggests that there is a rather wide range in the estimates of the inflection point where the rate changes direction. (Yu et al., 2013) reported that the same difference between the 100 nm and 400 nm size ranges was observed in the theoretically estimated deposition loss rate coefficient. However, they pointed out that aerosols with a broad size distribution may not be appropriate for calculating the deposition rate since larger particles have a considerable scavenging effect on relatively smaller particles. Nonetheless, the inflection points of broiled fish and incense derived from this study show that deposition rates can be calculated for some distributions and concentrations where coagulation might be ignored. In fact, it was verified through model prediction analysis that the simulated values, calculated by applying the deposition rates estimated in the same way between this study and the previous study, and the measured values were similar (Jeong et al., 2021). Although more explicit verification is needed to estimate deposition rates, these similarities support the idea that the method presented herein can be a good alternative for calculating the deposition rate of aerosols with a wide particle size distribution.

The FOE coagulation loss rates represent the average first-order loss rate due to coagulation. Although the six indoor sources have different size distributions, the FOE coagulation loss rates are generally higher for sources with larger number concentrations at smaller sizes. This means that the aerosol process due to coagulation, according to the size and number concentration, works similarly during the emission period. In the case of a candle with a large number concentration at a smaller particle size, the FOE coagulation loss rates were close to 30 h^{-1} in the 2–5 nm size range. In the case of the gas stove, it also showed higher coagulation loss rates in the small size range. In the candle and gas stove, particle gains occurred between 15–30 nm and 10–20 nm, respectively. The differences in particle number concentration and size distribution between the two emission sources were attributed to these results. For the remaining four indoor sources, coagulation loss rates of 0.5–2 h^{-1} were also observed near the size of 10 nm. The gain due to coagulation for clothes dryer, tea & toast, and broiled fish occurred in the size range of 15–40 nm, 30–50 nm, and 50–100 nm, respectively, due to the coagulation rate dependent on the size distribution. Incense, on the other hand, showed negligible gain due to coagulation when compared to the other five indoor sources, mainly because of bigger particle sizes and a relatively small total number concentration.

3.3. Size-resolved source emission rates for the indoor emission sources

The emission strengths of six indoor sources is presented in Fig. 4, which displays the size-resolved source emission rates. The emission rates were found to exhibit a size distribution similar to the size-resolved UFP number concentration shown in Fig. 2, especially during the initial emission period. The source emission rates ranged between 10^7 min^{-1} and 10^{12} min^{-1} for the six indoor sources. The candle showed the highest value of 4.25×10^{12} min^{-1} for the total source emission rate. Furthermore, the total UFP emission rates were 1.15×10^{13} min^{-1} for gas stove, 2.24×10^{12} min^{-1} for tea & toast, 2.18×10^{12} min^{-1} for clothes dryer, 1.87×10^{12} min^{-1} for broiled fish, and 1.89×10^{11} min^{-1} for incense.

The candle burning resulted in the largest source emission rates (ranging from 2.58×10^{11} to 4.25×10^{12} min^{-1}) in the size range of 2–3 nm. In the case of the gas stove, the highest source emission rates of 2.93×10^{11} to 3.46×10^{11} min^{-1} were observed for the size range of 4–6 nm. As for the incense, the smallest source emission rates of 4.79×10^9 to 5.94×10^9 min^{-1} were found in the size range of 110–140 nm. Table 1 provides a detailed information of the total UFP number concentration, total source emission rate, and GMD associated with the log-normal distribution for the six indoor sources.

He et al. (2004) reported emission rates for different cooking sources ranging between 0.35×10^{11} and 7.34×10^{11} min^{-1} for particle sizes >15 nm based on measurements in 15 houses in Brisbane. Similarly, Wallace et al. (2008) ; investigated source emission rates for three indoor sources (an electric stove, a gas stove, an electric toaster oven) at the instrumented test house located on the campus of the National Institute of Standards and Technology (NIST). Based on more than 150 tests, the source emission rates reported in the study ranged from 0.06×10^{12} to 1.4×10^{13} min^{-1} in the size range of 2–64 nm. Géhin et al. (2008) also examined the size-resolved UFP emission rate for 18 different activities (cooking, burning candle, computer printing, use of spray etc.). Like this present study, the study results revealed that the lowest number distribution mode was 6 nm for the candles. Consequently, all cooking activities in the study demonstrated similar

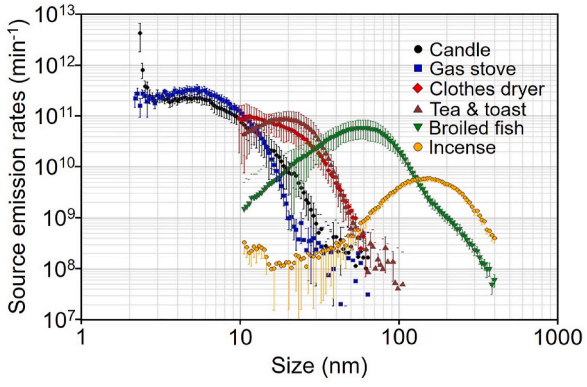

Fig. 4. Source emission rates for six indoor sources during emission period.

Table 1
Summary of total number concentrations, GMDs, and total source emission rates for the indoor emission sources.

Activity	Total number concentration at the start of decay (cm^{-3})	GMD at beginning of decay (nm), (GSD)	Total source emission rate (min^{-1})	GMD for total source emission rate (nm), (GSD)
Candle	310.1×10^4	Mode1: 2.34 (1.01) Mode2: 6.16 (1.84)	1.36×10^{13}	Mode1: 2.35 (1.01) Mode2: 4.91 (1.62)
Gas stove	30.5×10^4	5.92 (1.66)	1.15×10^{13}	4.82 (1.59)
Clothes dryer	7.25×10^4	17.26 (1.58)	2.18×10^{12}	15.92 (1.42)
Tea & toast	7.25×10^4	26.97 (2.61)	2.24×10^{12}	18.85 (1.38)
Broiled fish	24.2×10^4	47.01 (1.56)	1.87×10^{12}	51.51 (1.64)
Incense	2.12×10^4	128.14 (1.69)	1.89×10^{11}	133.01 (1.77)

emission in the 20–40 nm mode, and the observed total emission rate ranged between 0.06×10^{10} s^{-1} (3.6×10^{10} min^{-1}) and 13.10×10^{10} s^{-1} (7.86×10^{12} min^{-1}). In the literature review, it was determined that the emission rates are within a similar range (ranging from 0.06×10^{10} to 1.4×10^{13} min^{-1}) to this study. However, it should be noted that there may be potential discrepancies in the geometric mean diameter (GMD) and emission rates due to different experimental conditions and characteristics of the houses. Table 2 provides a summary of comparative analysis results of the source emission rates from literature, which reports GMDs (or mode) and size ranges observed with various indoor source activities. The source emission rate and GMD derived in this study are comparable to other studies. Although there was a difference in the source emission rate for each experiment, the GMDs (or modes) of candle burning, cooking activities, and incense burning in other studies were similar (3.2–180 nm) to those in the present study.

3.4. Contributions of coagulation, deposition and ventilation losses

Fig. 5 shows the concentration loss ratios due to coagulation, deposition and ventilation over the whole period (both emission and decay). The figure presents information on the major loss mechanisms at a specific time for each source. In the graph, the shaded parts with blue color represent the source emission period, while the transparent part shows the decay period. Overall, coagulation and deposition were dominant for candles and gas stoves with relatively high UFP number concentrations for sizes <10 nm. Note that the loss ratio due to coagulation notably increases during the emission period as the UFP number concentration rises and it remains high during the initial decay period. In the case of a candle with a high UFP number concentration (3.1×10^6 cm^{-3}), the rate of UFP number concentration loss due to coagulation gradually increased during the emission period and reached up to 60% at the end of emission. This ratio was the highest among the sources, and the loss due to coagulation was close to 40% even at the beginning of emission.

The total number concentration in the indoor space increased quickly because a number of small particles emitted from the candle diffused into a relatively small indoor space (25.8 m^3). Furthermore, for the candle, the particle loss due to coagulation and deposition was notably large because the ventilation rate was as low as 0.04 h^{-1}. In another study by Patel et al. (2021), the contributions of exfiltration, coagulation, and deposition to the number concentration were reported for sub-500 nm particles during breakfast and chili preparation over a 30-min period. They found that the loss fraction due to coagulation and deposition showed about 90% at the beginning of decay, and the loss due to coagulation was 40% for breakfast, which was four times greater than chili (10%). This trend was because the number concentration due to breakfast (2.4×10^5 cm^{-3}) was notably higher than that of chili (6.4×10^4 cm^{-3}), leading to more UFP number concentration loss due to coagulation. Wallace et al. (2019) calculated the contributions of coagulation, deposition, and ventilation to the decay of UFPs (2–64 nm) emitted from candles in indoor space. In this experiment, it was confirmed that the contribution of loss due to coagulation was 65% at the beginning of decay with a high concentration and decreased to 17% as the decay progressed. These previous study results agree well with this study, in which the contribution of UFP loss due to coagulation (65% of the total loss) and deposition (35% of the total loss) was dominant at the beginning of decay. Note that the number concentration loss due to ventilation was only 0.21% of the total loss. The concentration due to gas stove was 3.05×10^5 cm^{-3} at the end of the emission, while coagulation and deposition were responsible for 37% and 61% of the total particle loss, respectively. During the emission period, the loss rate of coagulation increased with the increase in number concentration for most of the source events. However, in the case of incense, both the emission period and the decay periods had relatively constant coagulation and deposition due to low number concentration (2.12×10^4 cm^{-3}) of large particles. Accordingly, the ventilation loss showed the

Table 2
The comparative analysis of the source emission rate, GMD (or mode) and observed size range according to various indoor source activities.

	Activity	GMD or Mode (nm)	Observed size range	Source emission rate (min^{-1})
He et al. (2004)	Cooking	–	>15 nm	5.67×10^{11}
	Cooking pizza	–	>15 nm	1.65×10^{11}
	Frying	–	>15 nm	4.75×10^{11}
	Grilling	–	>15 nm	7.34×10^{11}
Wallace et al. (2008)	Burner (Gas stove)	4.0–20	2–64 nm	$0.4–13 \times 10^{12}$
	Oven (Gas stove)	4.3–24	2–64 nm	$0.3–5.1 \times 10^{12}$
	Stovetop coil (Electric stove)	3.2–31	2–64 nm	$0.14–14 \times 10^{12}$
	Oven (Electric stove)	5.2–30	2–64 nm	$0.06–0.8 \times 10^{12}$
	Oven (Electric toaster oven)	16–49	2–64 nm	$1.8–6.4 \times 10^{12}$
Géhin et al. (2008)	White candle	around 170	5–1000 nm	$3.6–6.0 \times 10^{10}$
	Perfumed candle	around 6	5–1000 nm	$0.65–2.17 \times 10^{12}$
	Cooking activities (frying meat, frying fish, cooking pasta etc.)	20–40	5–1000 nm	$0.22–7.39 \times 10^{12}$
	Burning incense	100–180	5–1000 nm	$3.6–4.1 \times 10^{11}$
The present study	Candle	2.35, 4.91	2–64 nm	1.36×10^{13} (total)
	Cooking activities	4.82–51.51	2–400 nm	$0.19–1.15 \times 10^{13}$ (total)
	Incense	133.01	10–400 nm	1.89×10^{11} (total)

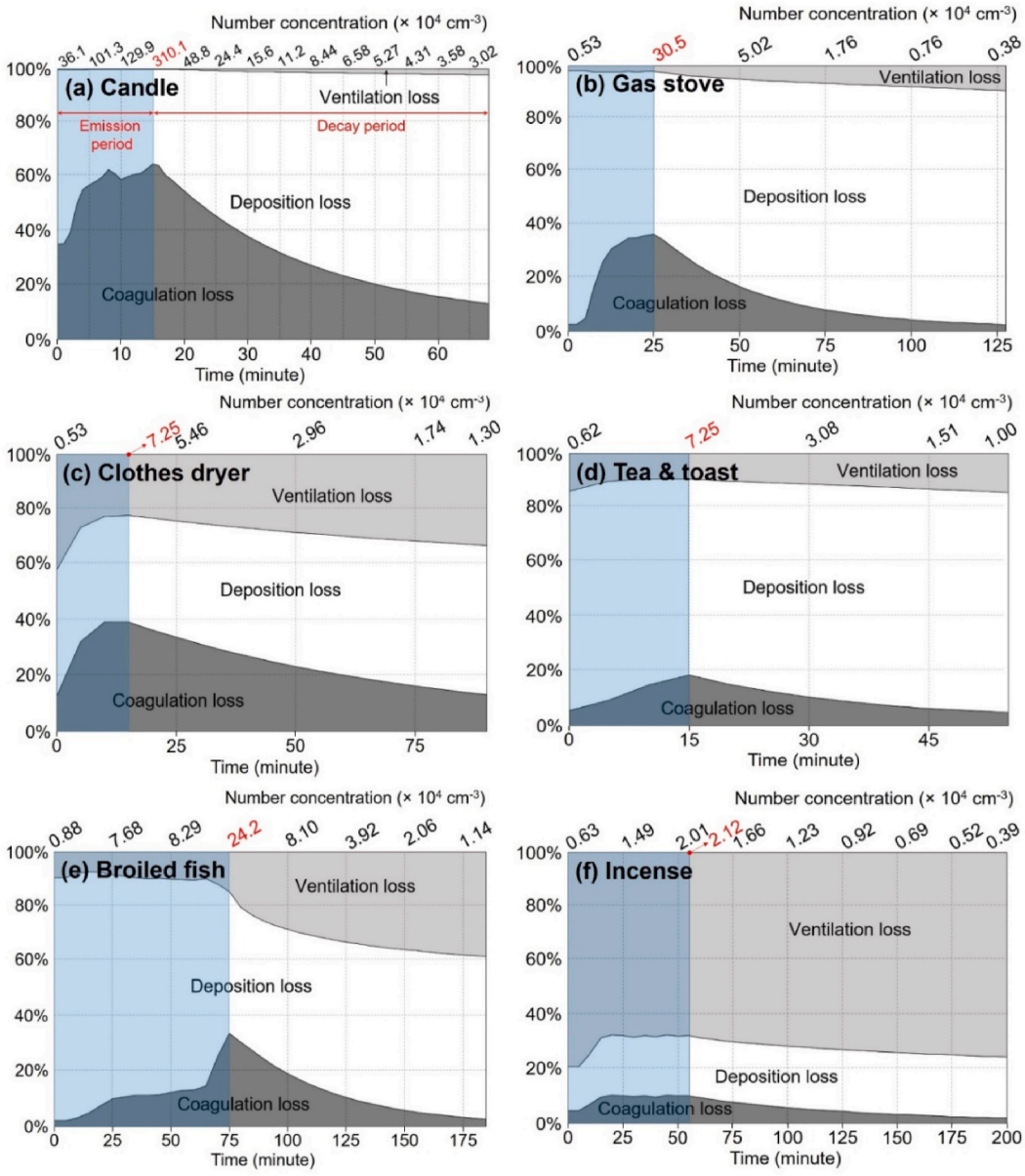

Fig. 5. Ratios of UFP number concentration loss due to coagulation, deposition and ventilation during emission and decay periods by sin indoor emission source.

highest (up to 80%) compared to other indoor sources. These results suggest that three aerosol loss mechanisms can meaningfully affect particle concentration and size distribution dynamics during the emission and decay periods, depending on the source type and environmental condition.

4. Conclusions

This study investigated size-resolved source emission rates and aerosol dynamic processes for six distinct indoor sources. Using experimental data, the present study 1) analyzed time-variations of size-resolved number concentrations and source emission rates for six indoor sources, 2) estimated the time-dependent coagulation and deposition loss rates, and 3) reported the relative contributions of coagulation, deposition and ventilation over the entire (i.e., emission and decay) period. This study demonstrates that coagulation and deposition are important aerosol dynamic processes during source emission that influence ultrafine particle size dynamics.

- As the emission progressed, particle number concentration increased while showing a log-normal distribution with the geometric mean increasing over time.
- Particle coagulation plays an important role in size and number concentration dynamics during the emission period. The particle coagulation losses are generally higher for emission sources with smaller sizes at larger number concentrations (i.e., candle & gas stove).
- The size-resolved emission rates can be expressed as log-normal distributions, while the different indoor sources show widely-varying emission rates ranging from 10^7 min^{-1} to 10^{13} min^{-1}. Candle burning showed the highest total emission rate of 1.36×10^{13} min^{-1} followed by the gas stove.
- Overall, the results suggest that for aerosol dynamics due to episodic indoor emission events, coagulation and deposition should be considered for estimating source emission rates for ultrafine particles.

Note that the main purpose of this study is to establish a particle

dynamic model that estimates size-resolved UFP emission rates, considering detailed the aerosol transformation processes during emission and decay periods. However, there are limitations in this study as we analyzed field experiment data collected from different locations at different times. While the variations in instrumentation and detection size range are partially reflected in the error bars in source emission rates and deposition rates, future studies are warranted to address this limitation by using laboratory experiment data collected with the same instruments in more controlled environments. Ultimately, using the aerosol transformation mechanisms examined in this study, researchers can refine exposure assessment for epidemiological studies on indoor ultrafine particles.

Author statement

Su-Gwang Jeong: Writing - review & editing, Visualization. **Lance Wallace:** Methodology, Resources. **Donghyun Rim:** Conceptualization, Supervision, Writing - review & editing.

Declaration of competing interest

The authors declare that they have no known competing financial interests or personal relationships that could have appeared to influence the work reported in this paper.

Data availability

Data will be made available on request.

Acknowledgement

The research presented in this paper was supported by the U.S. National Science Foundation (NSF Grant 1944325) and the Basic Science Research Program through the National Research Foundation of Korea funded by the Ministry of Education (NRF-2020R1A6A1A03044977).

Appendix A. Supplementary data

Supplementary data to this article can be found online at https://doi.org/10.1016/j.envpol.2023.122680.

References

Adeniran, J.A., Yusuf, R.O., Oke, E.O., 2019. Deposition and coagulation of aerosols from household spray products. Songklanakarin J. Sci. Technol. 41, 10–14456. https://doi.org/10.14456/sjst-psu.2019.25.

Amouei Torkmahalleh, M., Naseri, M., Nurzhan, S., Gabdrashova, R., Bekezhankyzy, Z., Gimnkhan, A., Malekipirbazari, M., Jouzizadeh, M., Tabesh, M., Farrokhi, H., 2022. Human exposure to aerosol from indoor gas stove cooking and the resulting nervous system responses. Indoor Air 32, e12983. https://doi.org/10.1111/ina.12983.

Anand, S., Sreekanth, B., Mayya, Y.S., 2016. Effective coagulation coefficient approach for estimating particle number emission rates for strong emission sources. Aerosol Air Qual. Res. 16, 1541–1547. https://doi.org/10.4209/aaqr.2015.10.0586.

Bhangar, S., Mullen, N., Hering, S., Kreisberg, N., Nazaroff, W., 2011. Ultrafine particle concentrations and exposures in seven residences in northern California. Indoor Air 21, 132–144. https://doi.org/10.1111/j.1600-0668.2010.00689.x.

Géhin, E., Ramalho, O., Kirchner, S., 2008. Size distribution and emission rate measurement of fine and ultrafine particle from indoor human activities. Atmos. Environ. 42, 8341–8352. https://doi.org/10.1016/j.atmosenv.2008.07.021.

Gao, N., Niu, J., 2007. Modeling particle dispersion and deposition in indoor environments. Atmos. Environ. 41, 3862–3876. https://doi.org/10.1016/j.atmosenv.2007.01.016.

Glytsos, T., Ondráček, J., Džumbová, L., Kopanakis, I., Lazaridis, M., 2010. Characterization of particulate matter concentrations during controlled indoor activities. Atmos. Environ. 44, 1539–1549. https://doi.org/10.1016/j.atmosenv.2010.01.009.

He, C., Morawska, L., Hitchins, J., Gilbert, D., 2004. Contribution from indoor sources to particle number and mass concentrations in residential houses. Atmos. Environ. 38, 3405–3415. https://doi.org/10.1016/j.atmosenv.2004.03.027.

Hinds, W.C., 1982. Aerosol Technology: Properties, Behavior, and Measurement of Airborne particles(Book). Wiley-Interscience, New York, p. 442, 1982.

Hussein, T., Glytsos, T., Ondráček, J., Dohányosová, P., Ždímal, V., Hämeri, K., Lazaridis, M., Smolík, J., Kulmala, M., 2006. Particle size characterization and emission rates during indoor activities in a house. Atmos. Environ. 40, 4285–4307. https://doi.org/10.1016/j.atmosenv.2006.03.053.

Hussein, T., Hruška, A., Dohányosová, P., Džumbová, L., Hemerka, J., Kulmala, M., Smolík, J., 2009. Deposition rates on smooth surfaces and coagulation of aerosol particles inside a test chamber. Atmos. Environ. 43, 905–914. https://doi.org/10.1016/j.atmosenv.2008.10.059.

Jeong, S.-G., Wallace, L., Rim, D., 2021. Contributions of coagulation, deposition, and ventilation to the removal of airborne Nanoparticles in indoor environments. Environ. Sci. Technol. 55, 9730–9739. https://doi.org/10.1021/acs.est.0c08739.

Koivisto, A.J., Kling, K.I., Hänninen, O., Jayjock, M., Löndahl, J., Wierzbicka, A., Fonseca, A.S., Uhrbrand, K., Boor, B.E., Jiménez, A.S., 2019. Source specific exposure and risk assessment for indoor aerosols. Sci. Total Environ. 668, 13–24. https://doi.org/10.1016/j.scitotenv.2019.02.398.

Koivisto, A.J., Yu, M., Hämeri, K., Seipenbusch, M., 2012. Size resolved particle emission rates from an evolving indoor aerosol system. J. Aerosol Sci. 47, 58–69. https://doi.org/10.1016/j.jaerosci.2011.12.007.

Lai, A.C., Nazaroff, W.W., 2000. Modeling indoor particle deposition from turbulent flow onto smooth surfaces. J. Aerosol Sci. 31, 463–476. https://doi.org/10.1016/S0021-8502(99)00536-4.

Laiman, R., He, C., Mazaheri, M., Clifford, S., Salimi, F., Crilley, L.R., Mokhtar, M.A.M., Morawska, L., 2014. Characteristics of ultrafine particle sources and deposition rates in primary school classrooms. Atmos. Environ. 94, 28–35. https://doi.org/10.1016/j.atmosenv.2014.05.013.

Li, H., Xu, D., Li, H., Wu, Y., Cheng, Y., Chen, Z., Yin, G., Wang, W., Ge, Y., Niu, Y., 2021. Exposure to ultrafine particles and oral flora, respiratory function, and biomarkers of inflammation: a panel study in children. Environ. Pollut. 273, 116489 https://doi.org/10.1016/j.envpol.2021.116489.

Li, L., Lin, Y., Xia, T., Zhu, Y., 2020. Effects of electronic cigarettes on indoor air quality and health. Annu. Rev. Publ. Health 41, 363. https://doi.org/10.1146/annurev-publhealth-040119-094043.

Nazaroff, W.W., 2008. Inhalation intake fraction of pollutants from episodic indoor emissions. Build. Environ. 43, 269–277. https://doi.org/10.1016/j.buildenv.2006.03.021.

Nazaroff, W.W., Cass, G.R., 1989. Mathematical modeling of indoor aerosol dynamics. Environ. Sci. Technol. 23, 157–166. https://doi.org/10.1021/es00179a003.

Ogulei, D., Hopke, P., Wallace, L., 2006. Analysis of indoor particle size distributions in an occupied townhouse using positive matrix factorization. Indoor Air 16, 204–215. https://doi.org/10.1111/j.1600-0668.2006.00418.x.

Ohlwein, S., Kappeler, R., Kutlar Joss, M., Künzli, N., Hoffmann, B., 2019. Health effects of ultrafine particles: a systematic literature review update of epidemiological evidence. Int. J. Publ. Health 64, 547–559. https://doi.org/10.1007/s00038-019-01202-7.

Or, V.W., Wade, M., Patel, S., Alves, M.R., Kim, D., Schwab, S., Grassian, V.H., 2020. Glass surface evolution following gas adsorption and particle deposition from indoor cooking events as probed by microspectroscopic analysis. Environ. Sci. Process. Impacts 22 (8), 1698–1709.

Ott, W.R., Zhao, T., Cheng, K.-C., Wallace, L.A., Hildemann, L.M., 2021. Measuring indoor fine particle concentrations, emission rates, and decay rates from cannabis use in a residence. Atmos. Environ. X 10, 100106. https://doi.org/10.1016/j.aeaoa.2021.100106.

Park, S., Lee, S., Yeo, M., Rim, D., 2023. Field and laboratory evaluation of PurpleAir low-cost aerosol sensors in monitoring indoor airborne particles. Build. Environ. 234, 110127 https://doi.org/10.1016/j.buildenv.2023.110127.

Patel, S., Rim, D., Sankhyan, S., Novoselac, A., Vance, M.E., 2021. Aerosol dynamics modeling of sub-500 nm particles during the HOMEChem study. Environ. Sci. J. Integr. Environ. Res.: Process. Impacts 23, 1706–1717. https://doi.org/10.1039/D1EM00259G.

Patel, S., Sankhyan, S., Boedicker, E.K., DeCarlo, P.F., Farmer, D.K., Goldstein, A.H., Katz, E.F., Nazaroff, W.W., Tian, Y., Vanhanen, J., 2020. Indoor particulate matter during HOMEChem: concentrations, size distributions, and exposures. Environ. Sci. Technol. 54, 7107–7116. https://doi.org/10.1021/acs.est.0c00740.

Rim, D., Choi, J.-I., Wallace, L.A., 2016. Size-resolved source emission rates of indoor ultrafine particles considering coagulation. Environ. Sci. Technol. 50, 10031–10038. https://doi.org/10.1021/acs.est.6b00165.

Rim, D., Green, M., Wallace, L., Persily, A., Choi, J.-I., 2012. Evolution of ultrafine particle size distributions following indoor episodic releases: relative importance of coagulation, deposition and ventilation. Aerosol. Sci. Technol. 46, 494–503. https://doi.org/10.1080/02786826.2011.639317.

Salthammer, T., Gu, J., Wientzek, S., Harrington, R., Thomann, S., 2021. Measurement and evaluation of gaseous and particulate emissions from burning scented and unscented candles. Environ. Int. 155, 106590 https://doi.org/10.1016/j.envint.2021.106590.

Siegel, J.A., Nazaroff, W.W., 2003. Predicting particle deposition on HVAC heat exchangers. Atmos. Environ. 37, 5587–5596. https://doi.org/10.1016/j.atmosenv.2003.09.033.

Slezakova, K., Pereira, M.C., Morais, S., 2020. Ultrafine particles: levels in ambient air during outdoor sport activities. Environ. Pollut. 258, 113648 https://doi.org/10.1016/j.envpol.2019.113648.

Wallace, L., 2006. Indoor sources of ultrafine and accumulation mode particles: size distributions, size-resolved concentrations, and source strengths. Aerosol. Sci. Technol. 40, 348–360. https://doi.org/10.1080/02786820600612250.

Wallace, L., Jeong, S.G., Rim, D., 2019. Dynamic behavior of indoor ultrafine particles (2.3-64 nm) due to burning candles in a residence. Indoor Air 29, 1018–1027. https://doi.org/10.1111/ina.12592.

Wallace, L., Kindzierski, W., Kearney, J., MacNeill, M., Héroux, M.-È., Wheeler, A.J., 2013. Fine and ultrafine particle decay rates in multiple homes. Environ. Sci. Technol. 47, 12929–12937. https://doi.org/10.1021/es402580t.

Wallace, L., Wang, F., Howard-Reed, C., Persily, A., 2008. Contribution of gas and electric stoves to residential ultrafine particle concentrations between 2 and 64 nm: size distributions and emission and coagulation rates. Environ. Sci. Technol. 42, 8641–8647. https://doi.org/10.1021/es801402v.

Wallace, L.A., Emmerich, S.J., Howard-Reed, C., 2004. Source strengths of ultrafine and fine particles due to cooking with a gas stove. Environ. Sci. Technol. 38, 2304–2311. https://doi.org/10.1021/es0306260.

Wang, C., Collins, D.B., Hems, R.F., Borduas, N., Antiñolo, M., Abbatt, J.P., 2018. Exploring conditions for ultrafine particle formation from oxidation of cigarette smoke in indoor environments. Environ. Sci. Technol. 52, 4623–4631. https://doi.org/10.1021/acs.est.7b06608.

Wierzbicka, A., Bohgard, M., Pagels, J., Dahl, A., Löndahl, J., Hussein, T., Swietlicki, E., Gudmundsson, A., 2015. Quantification of differences between occupancy and total monitoring periods for better assessment of exposure to particles in indoor environments. Atmos. Environ. 106, 419–428. https://doi.org/10.1016/j.atmosenv.2014.08.011.

Yu, M., Koivisto, A.J., Hämeri, K., Seipenbusch, M., 2013. Size dependence of the ratio of aerosol coagulation to deposition rates for indoor aerosols. Aerosol. Sci. Technol. 47, 427–434. https://doi.org/10.1080/02786826.2012.759640.

Zai, S., Zhen, H., Jia-song, W., 2006. Studies on the size distribution, number and mass emission factors of candle particles characterized by modes of burning. J. Aerosol Sci. 37, 1484–1496. https://doi.org/10.1016/j.jaerosci.2006.05.001.

Zhang, Q., Avalos, J., Zhu, Y., 2014. Fine and ultrafine particle emissions from microwave popcorn. Indoor Air 24, 190–198. https://doi.org/10.1111/ina.12069.

Zhao, Y., Wang, F., Zhao, J., 2015. Size-resolved ultrafine particle deposition and Brownian coagulation from gasoline vehicle exhaust in an environmental test chamber. Environ. Sci. Technol. 49, 12153–12160. https://doi.org/10.1021/acs.est.5b02455.